Journal of Rock Mechanics and Geotechnical Engineering 17 (2025) 8161–8171

Contents lists available at ScienceDirect

Journal of Rock Mechanics and Geotechnical Engineering

journal homepage: www.jrmge.cn

Full Length Article

Dilation on granular flows: Insight for friction weakening on debris avalanches

Yuxiang Hu [a], Congjiang Li [b], Qingyang Zhu [a], Haibo Li [b], Jiawen Zhou [a,c,*]

[a] State Key Laboratory of Hydraulics and Mountain River Engineering, Sichuan University, Chengdu, 610065, China
[b] College of Water Resources and Hydropower, Sichuan University, Chengdu, 610065, China
[c] Institute for Disaster Management and Reconstruction, Sichuan University-The Hong Kong Polytechnic University, Chengdu, 610200, China

ARTICLE INFO

Article history:
Received 9 October 2024
Received in revised form
8 July 2025
Accepted 21 August 2025
Available online 25 September 2025

Keywords:
Granular avalanches
Movement process
friction weakening
Physical experiments
Numerical simulation

ABSTRACT

Debris avalanches are a major concern due to their high mobility. However, the mechanism of friction weakening in debris avalanches remains poorly understood. This study systematically investigates the friction weakening mechanism of granular flows using rotation drum experiments, large-scale chute experiments, and numerical simulations. Notably, dilation of granular flows is a characteristic feature associated with friction weakening. The results indicate that dilation occurs synchronously with friction weakening during the motion of granular flows, as evidenced by the motion patterns and force interactions of debris avalanches. Collision contacts were identified as the primary driver of particle dilation. An optimal collision strength can induce dilation of granular flows, reducing contact between the sliding body and substrate, thereby leading to friction weakening. The peak collision strength of granular flows during movement is determined by fragment size. The critical condition for triggering friction weakening in debris avalanches is identified as the peak Savage number ($N_{s,p}$) greater than 1.06. A mathematical model based on the granular inertial collision-friction coupling equation was developed. This study provides compelling evidence that the fractal dimension of various types of high-speed debris avalanches tends to stabilize within a narrow range.

1. Introduction

Mountains host approximately 15% of the global population and are highly vulnerable to geological disasters. High-speed debris avalanches are one of the most destructive natural hazards in mountainous regions. Notably, these avalanches commonly exhibit friction weakening during movement, a critical phenomenon influencing their dynamics and destructive potential. The fragmented assembly does not lose mobility and can move several kilometers over horizontal ground (Cruden and Krahn, 1978; Davies and McSaveney, 2009). For example, on 29 April 1903, a giant landslide occurred in Alberta, Canada, resulting in the movement of 4×10^7 m^3 of debris avalanche material over a distance of 2.5 km in less than 30 s. This catastrophic event led to the burial of half of the town of Frank, claiming the lives of over 10,000 individuals (Cruden and Hungr, 1986). Some of the boulders in the accumulation displayed well-preserved edges, and objects such as undamaged tree trunks and house structures were found within, implying that the internal motion of the debris avalanche resembled that of a non-Newtonian fluid. Similarly, on 24 June 2017, a landslide of approximately 4.5×10^6 m^3 of debris avalanche occurred in Xinmo village, Sichuan Province, China. This landslide moved approximately 2.6 km in 60 s and resulted in 10 deaths and 73 people reported missing (Zhao et al., 2021).

The potential mechanisms of friction weakening include air lubrication, pore water liquefaction, and heating lubrication (McEwen, 1989; Legros, 2002; Staron and Hinch, 2007; Deline et al., 2011; Singer et al., 2012; Medwedeff et al., 2020; Li and Moon, 2021; Deng et al., 2023). The presence of a liquid phase at the sliding surface can provide a lubricating effect between the sliding mass and substrate. However, debris avalanches occurring on other planes or under completely dry conditions also exhibit enhanced mobility (Davies and McSaveney, 1999; Collins and

* Corresponding author. State Key Laboratory of Hydraulics and Mountain River Engineering, Sichuan University, Chengdu, 610065, China.
E-mail address: jwzhou@scu.edu.cn (J. Zhou).

Peer review under responsibility of Institute of Rock and Soil Mechanics, Chinese Academy of Sciences.

https://doi.org/10.1016/j.jrmge.2025.08.010

Melosh, 2003). A connection between temperature increase and friction weakening has been documented in coal-measure rock avalanches (Goren and Aharonov, 2007; Hu et al., 2018). The observed reduction in frictional resistance in mining areas during landslides may be attributed to chemical material transfer processes at the sliding interface. In contrast, landslide mobility enhancement in non-mining regions is likely controlled by physical mechanisms (Fisher, 1971; Campbell, 1989; Robinson et al., 2015). Therefore, a better understanding of the friction-weakening mechanisms of debris avalanches is necessary.

Debris avalanches are composed of discrete fragments and are accompanied by frequent energy transfer between fragments (Stark and Hovius, 2001; Frattini and Crosta, 2013). A particle-based mechanism is considered acceptable for explaining friction weakening. From the perspective of fragment fluctuations, rapidly increasing stress at the base of the slide can produce a sonic boom-like effect around the basement layer, helping to transition the slide into a fluidized state, thereby reducing friction (Yamada et al., 2018). Iverson and Vallance (2001) concluded that fragments alone in sliding masses, without the participation of other media, can cause debris avalanches to undergo a sudden reduction in friction. The interaction between mass flow and substrate reflects the internal processes that enhance movement, which is an important flow mobility and friction pattern manifestation (Hsu et al., 2008; Lucas et al., 2014; Allstadt et al., 2019; Bartali et al., 2020). A typical phenomenon observed in high-speed debris avalanches during the movement process is fluidization, in which larger fragments tend to move on the surface of the sliding mass as the entire avalanche moves in a flow-like manner (Davies, 1982; Johnson et al., 2015). However, these phenomena have not been completely reproduced or observed in experiments to verify the relation between friction weakening and fluidization. Therefore, further study of the debris avalanche movement process is necessary to identify the internal processes that enhance mobility.

Volume dilation of debris avalanches results from particle interactions (Cagnoli and Romano, 2012). Dilation is an important characteristic of frictional granular materials and is related to the evolution of topological structures within the granular assemblies (Walker and Tordesillas, 2010). The dilation of some fragments may reduce the contact between the sliding mass and substrate, which may suggest the occurrence of friction weakening. However, there is no evidence to illustrate that fragment dilation is related to the friction weakening of the sliding mass. In this study, a series of experiments was conducted to investigate the dilation effect of granular flows and its relationship with friction weakening. Our findings indicate that the dilation and friction weakening of debris avalanches are synchronous responses. More evidence of dilation and friction weakening was obtained through large-scale chute experiments. This study also discusses the critical factors influencing friction weakening and explains how granular dimension affects the behavior of high-speed debris avalanches.

2. Methodology

The rotation drum experiments, large-scale chute experiments, and discrete element method (DEM) simulations were conducted to study the friction weakening mechanism. The parameters used in these experiments are provided in Table A1 in Appendix A.

2.1. Rotation drum experiments

A rotational drum apparatus was employed to investigate the interfacial interactions between fragmented materials and the substrate under high-velocity shear conditions. The system, driven by an electric motor, allows precise control of angular velocity within a range of 0–80 rad/s (loading scheme is provided in Table C1 in Appendix C). The rotation drum was gradually accelerated until the granular flow reached a steady state with the drum. Two motion cameras were positioned at the front and back of the drum (Fig. 1). The initial granular flow volume was kept uniform ($V_0 = 1400\ \mathrm{cm}^3$) in each experimental condition. A total of eight different granular sizes were tested (spherical material, with the density $\rho = 1500\ \mathrm{kg/m}^3$ and the granular particle diameter d_p = 1.5 mm, 2 mm, 2.5 mm, 3 mm, 4 mm, 5 mm, 6 mm, and 8 mm), representing debris avalanche fragments. A comprehensive overview of the conditions is provided in Table 1. The angular velocity was increased in a gradient loading scheme by 0.1 Hz, equivalent to 0.293 rad/s. The drum was rotated for 1 min to reach a stable status at each angular velocity condition.

Furthermore, a collapse experiment was conducted to determine the static friction coefficient of the granular flow. The total volume of the granular flow was precisely 400 cm^3. The granular materials were loaded into the column, with the bottom being covered by coarse paper. The hollow cylinder was lifted at a constant velocity under each condition. The initial granular column and the collapsed granular mass under different values of D and d are shown in Fig. 2. All experimental conditions are presented in Table 1.

2.2. Large-scale chute experiments

A large-scale experimental chute was employed to investigate the dilation phenomena based on forceful data. The experimental chute consisted of a hopper, an acceleration section, and a deposition section. The granular flow was transferred from the hopper while maintaining the same total mass. The experimental setup comprised three force sensors (range: 50 N; precision: 0.05 N;

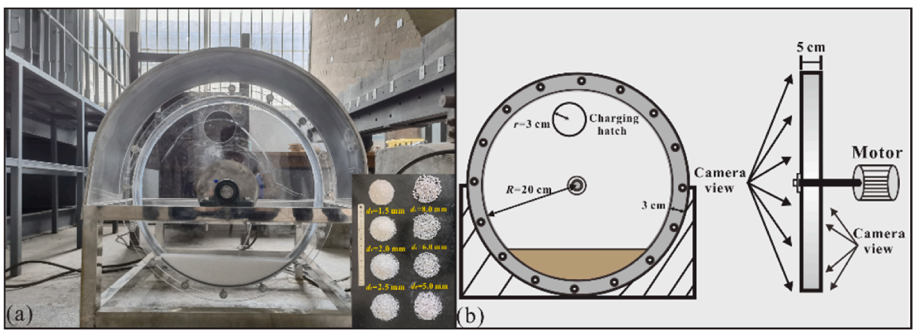

Fig. 1. Sketch of the rotation drum experiments: (a) Model of the rotation drum experiment; and (b) Detailed size of the experimental apparatus.

Table 1
Physical parameters of the rotation drum experiment and the static friction coefficient (μ_o) obtained through the collapse experiments (D is the fractal dimension, and d is the relative particle diameter).

No.	D	μ_o	No.	d	μ_o
1	0.55	0.24	1	0.04	0.29
2	1.18	0.25	2	0.03	0.33
3	1.56	0.3	3	0.025	0.33
4	1.85	0.34	4	0.02	0.34
5	2.30	0.37	5	0.015	0.38
6	2.66	0.36	6	0.0125	0.36
7	2.83	0.35	7	0.01	0.4
8	3	0.34	8	0.0075	0.43
9	3.34	0.37		–	
10	3.71	0.37			
11	4.15	0.37			
12	4.83	0.4			

diameter: 0.1 m), three thickness sensors (range: 1000 mm; precision: 0.1 mm), one microseismic sensor, two motion cameras (resolution: 2K, 240 fps), and one high-speed camera (resolution: 1080p, 1000 fps) (Fig. 3). Four different granular sizes were utilized, with $d_p = 6$ mm, 8 mm, 10 mm, and 20 mm (spherical material, with the density $\rho = 2500$ kg/m^3). The mass of the sliding material was 100 kg under all conditions. The detailed conditions of the large-scale chute experiments are summarized in Table 2.

2.3. Numerical simulations

DEM simulations were conducted based on large-scale chute experiments with experimental conditions of Nos. 1 and 5. The DEM simulations employed the Herz-Mindlin contact model, which does not consider the cohesion between particles. This contact model combines Herzen's normal force model and tangential force model developed by Mindlin and Deresiewicz (1953). The contact interactions between particles were modeled using the Hertz-Mindlin contact model. The governing equations for the normal force (F_n) and tangential force (F_t) between particles are expressed as follows:

$$F_n = \frac{4}{3}E^*\sqrt{R^*}\delta_n^{\frac{3}{2}} \tag{1}$$

$$F_t = -8G^*\sqrt{R^*\delta_n}\delta_t \tag{2}$$

where E^* is the equivalent Young's modulus; G^* is the equivalent shear modulus; R^* is the equivalent radius; and δ_n and δ_t represent the normal and tangential overlaps between particles, respectively.

The rolling friction torque (τ_i) is defined as

$$\tau_i = -\mu_r F_n R_i \omega_i \tag{3}$$

where μ_r is the rolling coefficient; R_i is the radius of contact particle i, and ω_i is the angular velocity of particle i.

The friction damping forces in the normal (F_n^d) and tangential (F_t^d) directions are given by

$$F_n^d = -2\sqrt{\frac{5}{6}}\beta\sqrt{S_n m^*}v_n\overrightarrow{rel} \tag{4}$$

$$F_t^d = -2\sqrt{\frac{5}{6}}\beta\sqrt{S_t m^*}v_t\overrightarrow{rel} \tag{5}$$

where β is the damping coefficient; S_n and S_t are the normal and tangential stiffness, respectively; m^* is the equivalent mass; and $v_n\overrightarrow{rel}$ and $v_t\overrightarrow{rel}$ are the normal and tangential components of the relative velocity between particles, respectively

The normal stiffness (S_n) and tangential stiffness (S_t) are calculated as

$$S_n = 2E^*\sqrt{R^*\delta_n} \tag{6}$$

$$S_t = 8G^*\sqrt{R^*\delta_n} \tag{7}$$

The numerical simulations were validated using time–space

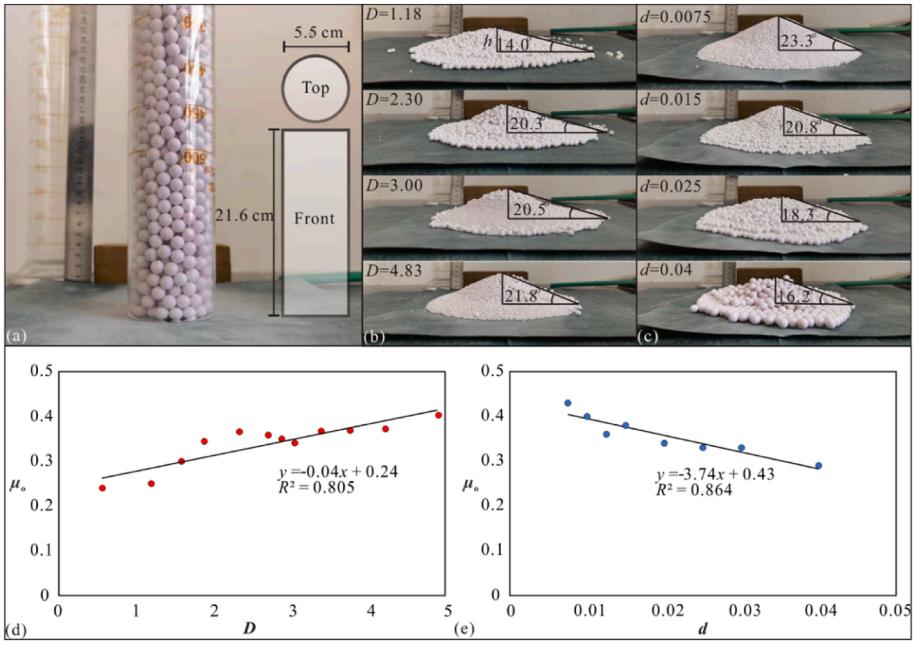

Fig. 2. Collapse experiments under varying granular compositions: (a) Hollow cylinder used in collapse experiments; (b) Static friction angle of granular flow under different values of D; (c) Static friction angle of granular flow under different values of d; (d) Fitting curve between μ_0 and D; and (e) Fitting curve between μ_0 and d.

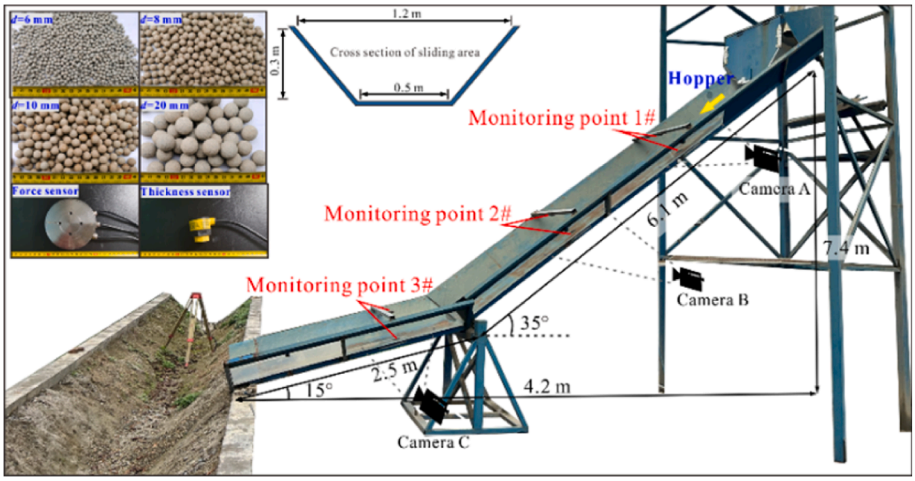

Fig. 3. Sketch of large-scale chute physical experiment.

Table 2
Physical parameters used in the large-scale chute experiments (d_1 is the diameter of fine particles, d_2 is the diameter of coarse particles, m_1 is the mass of fine particles, and m_2 is the mass of coarse particles).

No.	d_1 (mm)	d_2 (mm)	m_1 (kg)	m_2 (kg)	D
1	6	20	25	75	2.09
2	8	20	25	75	1.8
3	10	20	25	75	1.42
4	6	20	50	50	3
5	6	20	75	25	3.91

image information and velocity data obtained from three experimental monitoring points. The validated simulation parameters are presented in Table 3.

2.4. Definition of key parameters

To describe the particle size distribution of the sliding material, the relative particle size (d) is used to quantify the single particle size distribution:

$$d = \frac{d_p}{r} \tag{8}$$

where r is the rotation drum radius.

The mixed particle size distribution is described through the power-law particle size distribution, which is applied to study granular mobility in both experiments and numerical simulations, generated relative to a reference grain size d:

$$\frac{N(d_p)}{N_o} = \left(\frac{d_p}{d_o}\right)^{-D} \tag{9}$$

where $N(d_p)$ is the number of grains with diameter d_p, N_o is the number of grains with diameter d_o, and D is the power-law exponent called fractal dimension. A larger fractal dimension indicates that the number of fine particles is larger than that of the coarse particles.

In rotation drum experiments, the apparent friction coefficient is defined as the tangent of the inclination angle of the granular flow (Fig. 4a):

$$\mu^* = \tan\theta \tag{10}$$

The expansion coefficient (S^*) is determined from the rotation drum experiments and describes the enlarged area of the granular material under various conditions compared to the initial

Table 3
Parameters used in the numerical simulation.

Parameter	Value
Poisson's ratio of the fragments, λ_f	0.25
Density of the fragments, ρ_f (kg/m^3)	2500
Shearing modulus of the fragments, E (GPa)	10
Poisson's ratio of the chute, λ_c	0.3
Density of the chute, ρ_c (kg/m^3)	7900
Shearing modulus of the chute, E (GPa)	60
Restitution coefficient (fragment to fragment), $e_{f\text{-}f}$	0.2
Static friction coefficient (fragment to fragment), $f_{s,\,f\text{-}f}$	0.2
Rolling friction coefficient (fragment to fragment), $f_{r,\,f\text{-}f}$	0.1
Restitution coefficient (fragment to chute), $e_{f\text{-}c}$	0.2
Static friction coefficient (fragment to chute), $f_{s,\,f\text{-}c}$	0.3
Rolling friction coefficient (fragment to chute), $f_{r,\,f\text{-}c}$	0.1

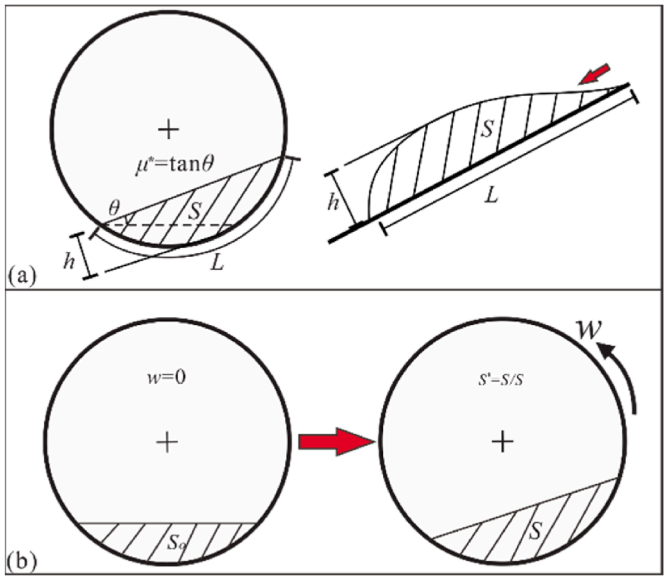

Fig. 4. Definition of parameters used in experiments: (a) The area of granular flow S, the contact length L, the apparent height h, and the apparent friction coefficient μ^*; and (b) The expansion coefficient S^*.

conditions (Fig. 4b). It is calculated as follows:

$$S^* = \frac{S}{S_o} \tag{11}$$

where S is the granular flow area under dynamic conditions, and S_o is its initial area under static conditions.

In large-scale chute experiments, the dynamic friction coefficient (μ) is used to quantify the friction of the sliding mass during movement, which is calculated based on the ratio of time-averaged force components:

$$\mu = \frac{\int_{t_0}^{t_e} F_s \mathrm{d}t}{\int_{t_0}^{t_e} F_n \mathrm{d}t} \tag{12}$$

where F_s and F_n are the shear and normal forces of debris avalanches, respectively; t_0 and t_e are the time recorded at the initial and final points.

Furthermore, the Savage number (N_s) is utilized to quantify the influence of particle behavior under various particle size distributions on the flow regime (Lai et al., 2017). N_s indicates the predominant particle behavior (collision or shearing) in granular mixtures. A larger N_s value implies a more pronounced collision interaction.

$$N_s = \frac{\dot{\gamma}^2 \overline{d}^2}{\mu_0 g h} \tag{13}$$

where μ_0 represents the static friction coefficient; $\dot{\gamma}$ denotes the shear rate of the granular material along the basement layer, and it can be calculated as $\dot{\gamma} = v/H^*$, in which v is the relative velocity; the parameter ($\overline{d}$) corresponds to the average particle size of the granular material, which can be determined through the weighted average $\overline{d} = (m_1 d_1 + m_2 d_2)/(m_1 + m_2)$, where m_1 and m_2 represent the particle masses with diameters d_1 and d_2, respectively; and h indicates the apparent height of the granular system. Additionally, the equivalent thickness, H^*, is a key parameter characterizing the frictional interaction between the granular material and the substrate. This dimensionless quantity is mathematically defined as the ratio of the granular flow's area (S) to its contact length (L) with the substrate, expressed as $H^* = S/L$. The data of contact length (L) and area (S) can be found in Tables C2–C4 in Appendix C.

3. Results

3.1. Particle dilation in rotation drum experiments

Photographic results from the rotation drum experiments indicate that the granular flow exhibits dilation as the movement velocity increases (Fig. 5a–f). The expansion coefficient (S^*) exhibits a positive response to the velocity of the granular flow (Fig. 5g), while the apparent friction coefficient (μ^*) is negatively influenced by the velocity of the granular flow (Fig. 5h). Generally, high-speed debris avalanches tend to show flow-like behavior under shearing effects. However, the dilation observed in granular flow is not a common characteristic of the movement of debris avalanches induced by shearing effects, as the interstices among granular particles become apparent under dilation. The motion pattern of the granular flow also includes intermittent bouncing, which is strongly related to the friction weakening in high-speed debris avalanches.

Additionally, granular flows comprising larger fragments exhibit greater dilation under the same external dynamic conditions (see Fig. 6a–c for slow dynamic conditions and Fig. 6d–g for rapid conditions). The fragment size is a critical factor in determining whether the sliding mass can undergo friction weakening. The granular flow with larger fragments shows higher N_s values under the same external dynamic conditions (Fig. 6h), and the apparent friction coefficient (μ^*) is negatively correlated with the Savage number (N_s) (Fig. 6i). The effect of shear rate on the mobility of granular flow is shown in Fig. 6j. It can be observed that as the shear rate increases, the friction coefficient of the granular flow increases only under certain particle size conditions (d = 0.0125, 0.02, and 0.04), and it remains largely unchanged under other conditions. Overall, the influence of shear rate on the mobility of granular flow is relatively minor.

To further analyze the experimental results, a correlation analysis was conducted between the Froude number (F_r) and apparent friction coefficient (μ^*), the dilation coefficient (S^*) and apparent friction coefficient (μ^*), as well as the Savage number (N_s) and apparent friction coefficient (μ^*). This enabled a quantitative evaluation of the degree of association between each dynamic parameter and the friction coefficient. The correlation analysis was performed using the Pearson correlation coefficient method:

$$r = \frac{\sum (x_i - \overline{x})(y_i - \overline{y})}{\sqrt{\sum (x_i - \overline{x})^2 \sum (y_i - \overline{y})^2}} \tag{14}$$

where x_i and y_i represent the ith observations of the two datasets, and $\overline{x}$ and $\overline{y}$ denote the mean values of the two datasets. Correlation analysis shows that the correlation coefficients (r) between the apparent friction coefficient (μ^*) and the Froude number (F_r), expansion coefficient, and the Savage number (N_s) are 0.041, −0.187, and −0.404, respectively (specific data are provided in Table C5 in Appendix C). This indicates that the apparent friction coefficient (μ^*) is primarily influenced by the Savage number (N_s), followed by the expansion coefficient (S^*). The results of the rotating drum experiments demonstrate that collision interactions dominate among larger fragments and serve as the primary dilation mechanism.

3.2. Particle dilation on large-scale chute experiments

Dilation of granular flow is a typical characteristic when friction weakening occurs in such flows. However, direct data obtained from rotation drum experiments were not sufficient to support the relationship between dilation and friction weakening. Therefore, detailed data on the normal and shear force during granular flow movement were obtained via large-scale chute experiments. The results show that dilation of the sliding mass is also observed during movement. The amplitude of dilation increases as the fractal dimension (D) decreases (Fig. 7a–c). At monitoring point #1, the peak shearing force decreases as the D decreases, and the data obtained from monitoring point #3 exhibit the same increasing tendency (Fig. 7d). The peak normal force remains constant (Fig. 7e), and the peak vibrating acceleration is positively correlated with the granular dimension. The sliding mass containing larger fragments shows a larger fluctuating vibration amplitude (Fig. 7f). The dynamic friction coefficient (μ) exhibits the same tendency as the variation in the granular dimension (Fig. 7g), which is synchronized with the amplitude of dilation under different fractal dimensions (Fig. 7a). The detailed force data obtained from large-scale chute experiments are presented in Fig. B1 in Appendix B.

In the numerical simulations, 15 additional monitoring points were set on the chute to investigate variations in the tangential and normal forces (Fig. 8a). The results were validated using time-space image information (Fig. 8b) and velocity data from physical

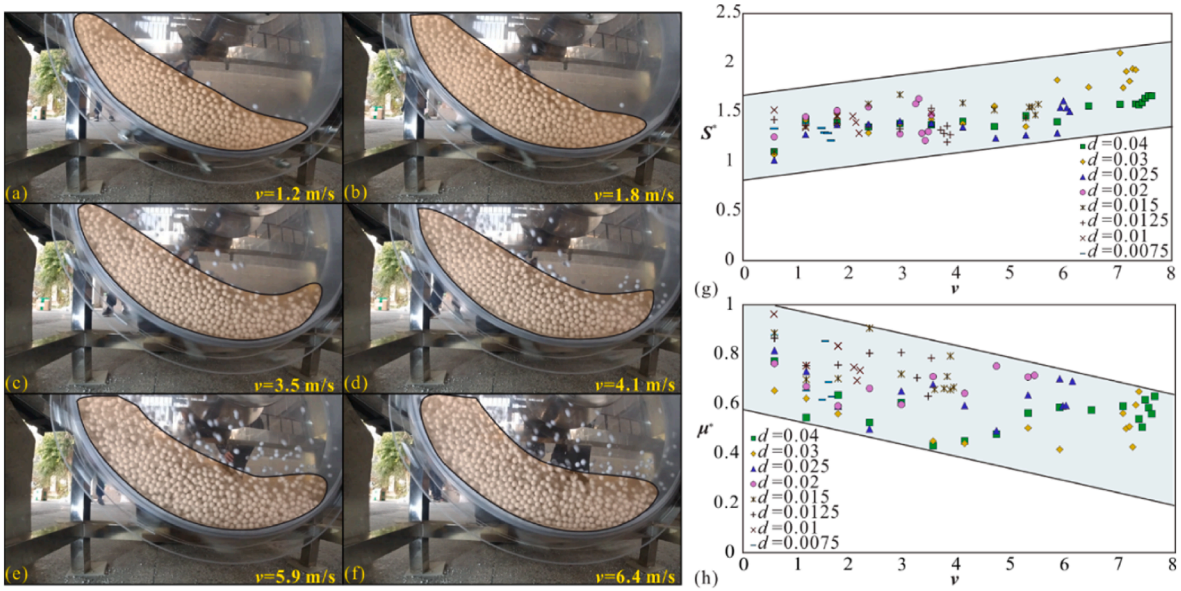

Fig. 5. Dilation observed in rotation drum experiments: (a–f) Motion pattern of granular flow under different velocity conditions with $d = 0.04$ in rotation drum experiments: (a) $v = 1.2$ m/s, (b) $v = 1.8$ m/s, (c) $v = 3.5$ m/s, (d) $v = 4.1$ m/s, (e) $v = 5.9$ m/s, and (f) $v = 6.4$ m/s; (g) Expansion coefficients corresponding to different velocity conditions; and (h) Apparent friction coefficient under velocity conditions.

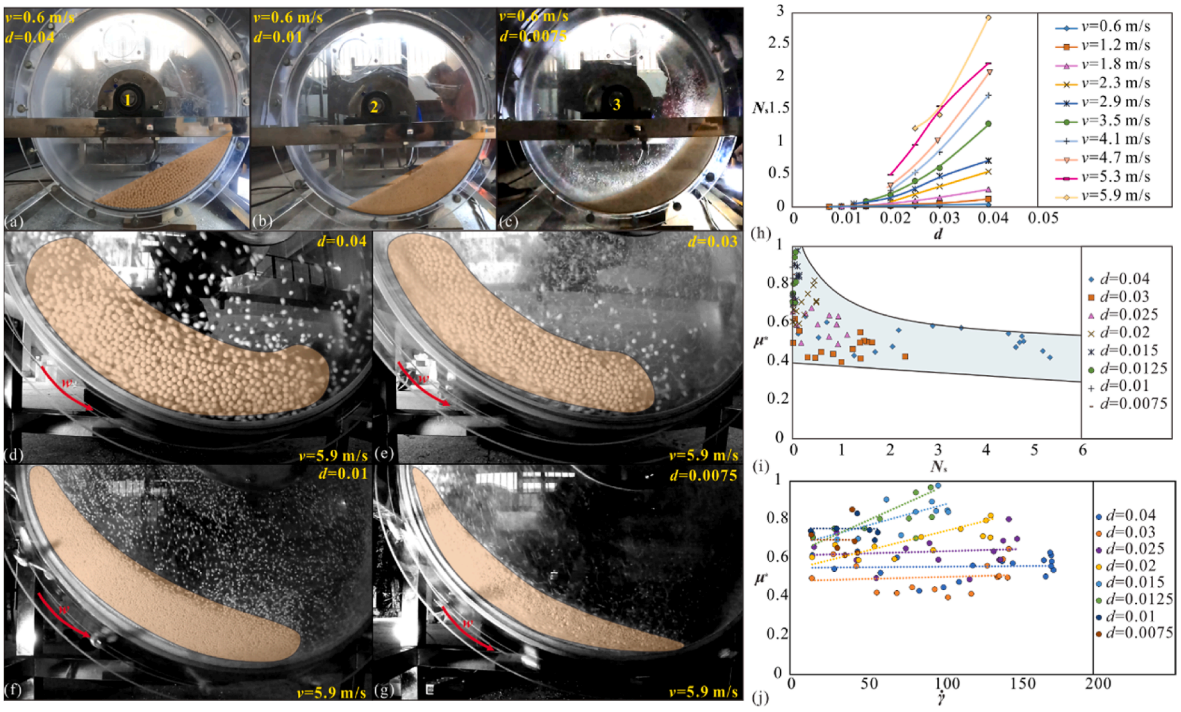

Fig. 6. Granular flow containing larger fragments exhibit smaller apparent friction coefficient: (a–c) Profile of granular flow under $d = 0.0075$, 0.01 and 0.04 with smaller velocity of $v = 0.6$ m/s; (d–g) Profile of granular flow under $d = 0.0075$, 0.01, 0.03 and 0.04 with larger velocity of $v = 5.9$ m/s; (h) Savage number is positively related to the fragment size of granular flow; (i) Dynamic friction coefficient decrease as the Savage Number increases; and (j) Dynamic friction coefficient does not change significantly as the increase of shear rate.

experiments (Fig. 8c–e). The numerical simulation results show that the tangential and normal forces decrease as the Savage number (N_s) increases. However, the amplitude of decrease in the normal force is significantly greater at $D = 2.09$, which further demonstrates that the sliding mass containing larger fragments exhibits extra dilation (as the normal force rapidly decreases with increasing N_s) due to the increase in collision contacts (Fig. 9).

4. Discussion

4.1. Critical influencing factor of friction weakening

The findings from the above-mentioned physical experiments indicate a close relationship between friction weakening and granular flow dilation; that is, the occurrence of dilation indicates

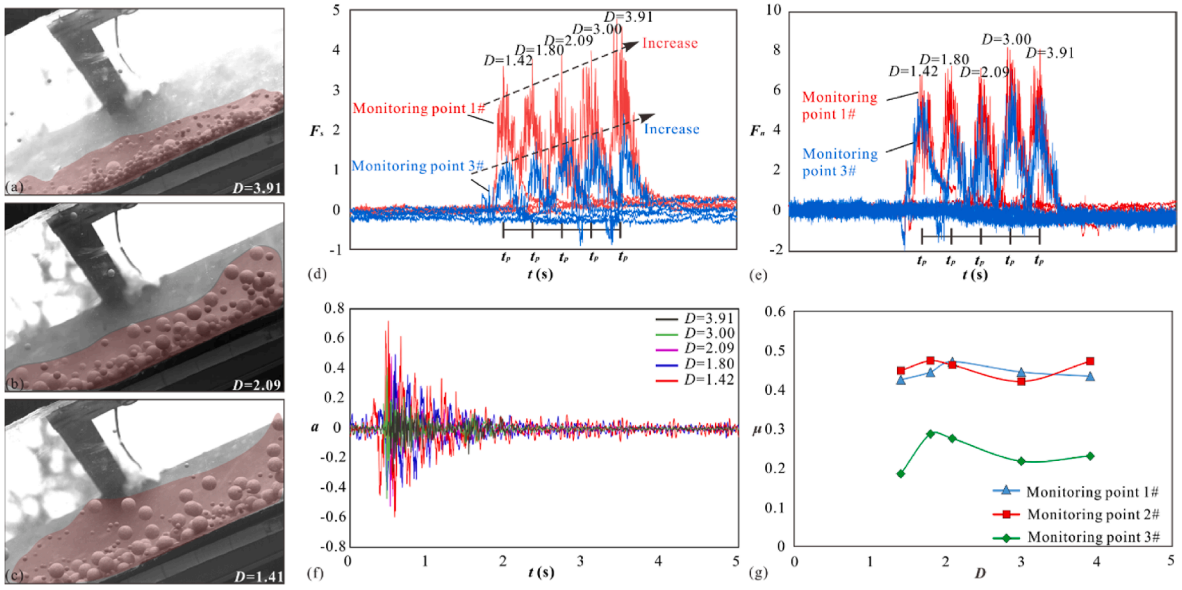

Fig. 7. Results of large-scale chute experiments: (a–c) Motion patterns of the granular flow under different particle size conditions in large-scale chute experiments: (a) $D = 3.91$, (b) $D = 2.09$, and (c) $D = 1.41$; (d) Peak shear force under fractal dimension corresponding to monitoring points #1 and #3; (e) Peak normal force under fractal dimension corresponding to monitoring points #1 and #3; (f) Vibrating acceleration under different fractal dimension; and (g) Dynamic friction coefficient under different fractal dimensions.

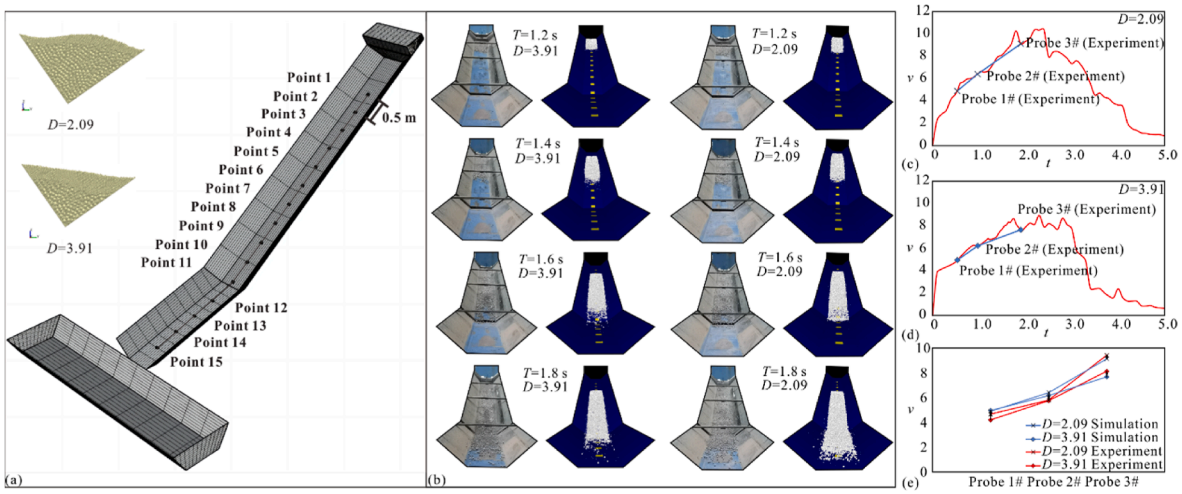

Fig. 8. DEM simulation model of large-scale chute experiment conducted through EDEM 2021: (a) Two conditions are conducted on simulation ($D = 2.09$ and $D = 3.91$) and 15 monitoring points are set (0.5 m interval each point); (b) Model validation based on movement process; (c) Model validation based on velocity data of sliding masses under $D = 2.09$; (d) Model validation based on velocity data of sliding masses under $D = 3.91$; and (e) Comparison with experimental probes.

a decrease in friction. This raises the following question: What mechanism causes particle dilation in granular flow? From the perspective of force interaction, dilation is the result of contacts within the granular flow. Previous studies have emphasized that the shear interaction is important for inducing forces that make the sliding mass move like a fluid, and the particle dilation can be explained by the shearing effect. However, the evolutionary trends of the peak shear force and the dynamic friction coefficient align under the same conditions in large-scale experiments. Consequently, the shear interaction may not contribute to dilation during the movement of the granular flow, nor does it support frictional weakening. Meanwhile, the collision contact between particles is another pivotal interaction mechanism in granular flow. It can therefore be speculated that the dilation is triggered by a collision.

The apparent friction coefficient and the dynamic friction coefficient are negatively correlated with the Savage number (N_s). The friction coefficient decreases gradually as the Savage number increases (Fig. 10a), indicating that the strength of the collision contact is related to the granular flow friction, rather than the shearing effect. Furthermore, the simulation results show that the peak shear and normal forces decrease as the Savage number increases, but the decrease in the amplitude of the peak normal force is substantially greater at $D = 2.09$ (see Fig. 9). This demonstrates that the sliding mass containing larger fragments exhibits enhanced dilation, with the normal force rapidly decreasing as the Savage number (N_s) increases due to increased collision contacts. The "D-based" increasing tendency of the collision contact is not influenced by variations in velocity. The dynamic friction coefficient is positively correlated with particle size, and this

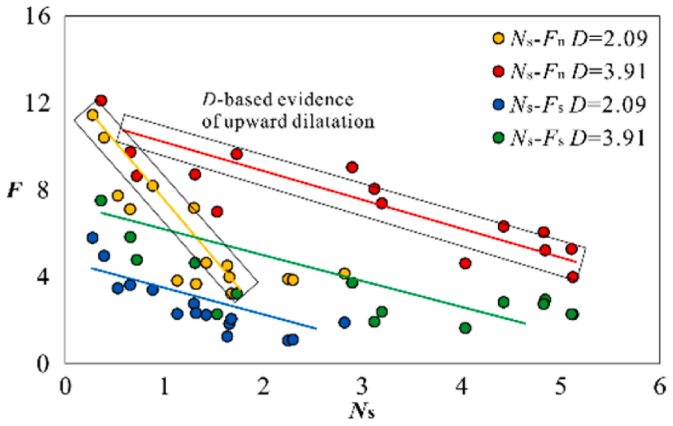

Fig. 9. Force data obtained by simulations. The peak normal and shear forces decrease as the Savage number increases, and the normal force sharply decreases at $D = 2.09$ compared with the condition of $D = 3.91$.

relationship can be observed under different velocity conditions. Granular flows with larger particle sizes demonstrate stronger collision contacts under the same external conditions, making them more likely to exhibit friction weakening. This is because granular flows containing larger fragments attain a higher Savage number (N_s) under the same external dynamic conditions.

The velocity condition and fragment size influence collision. A distinctive attribute of debris avalanches is their high mobility, which depends on external dynamic conditions. Another key characteristic is an internal factor: the fragment size, which plays a critical role in determining whether the sliding mass can experience friction weakening. To illustrate this, the peak Savage number ($N_{s,p}$) – defined as the Savage number under the critical rotation angular velocity of the granular flow – was calculated for different fractal dimensions (D) based on rotation drum experiments. The critical angular velocity associated with each D was also recorded to represent the dynamic friction of the granular flow. A larger critical angular velocity indicates that the granular assembly is subjected to less friction under the same external conditions (if the contact between the granular assembly and substrate is smooth, the critical angular velocity is infinite). The results show that the peak Savage number ($N_{s,p}$) decreases nonlinearly with increasing D. This indicates that the peak collision contact of the granular flow is restricted by the fractal dimension and that the particle contact tends to transform into shear interactions among fragments as the fragment size decreases (Fig. 10b). The characteristic point at which the critical angular velocity starts to decrease sharply is identified at a fractal dimension $D = 2.65$ with the corresponding peak Savage number $N_{s,p} = 1.06$. The point $N_{s,p} = 1.06$ serves as the demarcation point between collision- and shear-dominating effects in the movement process. When shear contact is the dominant mode of interaction between fragments ($N_{s,p} < 1.06$), friction rapidly increases. The D constrains the peak Savage number; when $D > 2.65$, the shear effect dominates the movement process, and $N_{s,p}$ remains small and is not influenced by variations in dynamic conditions. As a result, an increase in movement speed is insufficient to induce friction weakening when $D > 2.65$. Conversely, when $D < 2.65$, the collision effect gradually becomes dominant with increasing velocity (the peak $N_s > 1.06$) to trigger friction weakening. Therefore, the critical factor influencing friction weakening is fragment size, and two conditions are required to trigger friction weakening: (1) a fractal dimension $D < 2.65$, which is the basic condition (fragment size); and (2) sufficient momentum to support the generation of dilation (collision condition).

To further quantify the findings of this study, a mathematical model based on the granular inertial collision–friction coupling equation was established, linking collision intensity, degree of dilation, and basal friction coefficient. The basal friction coefficient is influenced by both the reduction in contacts due to dilation and the enhancement of collision effects and can be expressed as $\mu_c = f(\mu_0, S/S_0, N_s)$. Based on the fitting calculations using data from the rotating drum experiments, the following relationship was obtained:

$$\mu_c = \frac{1 + 3\mu_0(S^* - 1)}{2(1 + N_s)} \tag{15}$$

where μ_0 is the static friction coefficient, S^* is the expansion coefficient, and N_s is the Savage number.

A comparison between the apparent friction coefficient (μ^*) derived from experimental data and the calculated apparent friction coefficient (μ_c) is shown in Fig. 11. Both data sets are located near the function $\mu^* = \mu_c$, within a ±30% deviation range indicated by the dashed lines. This observation demonstrates that the model can be used to quantitatively analyze the relationship among collision, dilation, and frictional weakening.

4.2. Mechanism of friction weakening triggered by dilation

The mechanism of friction weakening in granular flows involves the interaction of collisions, which induces dilation. This, in turn, results in a reduction in contact between the whole sliding

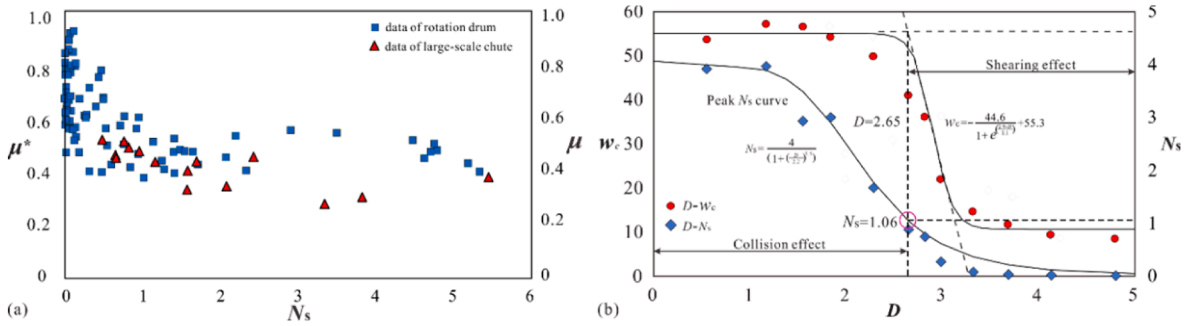

Fig. 10. Relationships between collision contact and friction weakening and between collision contact and fragment size: (a) The friction coefficient decreases as the Savage number increases in both kinds of experiments considered in this work; (b) The peak Savage number of the sliding mass is influenced by the fractal dimension (a curve fitted by a logistic function with $R^2 = 0.987$, the root mean square error (RMSE) = 0.214, and $N_s = 4/[1 + (D/2.2)^{5.5}]$) and the critical Savage number is 1.06. The critical angular velocity is also influenced by the fractal dimension (a curve fitted by a Boltzmann function with $R^2 = 0.99$, RMSE = 2.107, and $w_c = 44.6/[1 + e^{(2.9-D)/0.1}] + 55.3$), corresponding to a critical fractal dimension of 2.65.

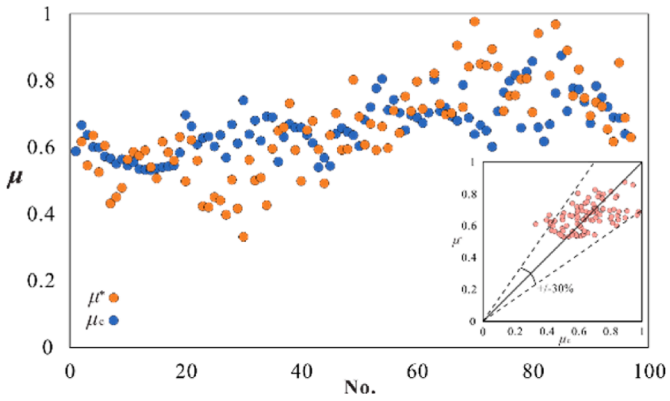

Fig. 11. The relations between experimental (μ^*) and calculated (μ_c) apparent friction coefficients.

mass and the substrate. The essential mechanism contributing to friction weakening is the collision of particles. The size discrepancy of the fragments determines the peak collision strength of the granular flow. Granular flows containing larger fragments can better acquire momentum and exhibit lower friction through collision contact (Fig. 12a). Furthermore, the dilation effect tends to cause large fragments to gradually move to the surface, finally depositing at the top of the sliding mass. Such accumulations of large fragments have been identified on deposition surfaces during field investigations of high-speed debris avalanches (Fig. 12b–d).

At the initial stage of movement, the fractal dimension of debris avalanches is relatively small because the sliding masses are not yet fully fragmented. Friction weakening can be triggered rapidly by collision contact as the velocity of the debris avalanche increases during movement. However, strong collision contacts lead to greater fragmentation of the sliding mass, which increases the fractal dimension, ultimately resulting in the fractal dimension exceeding the critical fractal dimension. The peak Savage number tends to decrease and remains at a lower value, and the friction weakening gradually ceases. With increasing fractal dimension, the collision effect gradually weakens, and the subsequent fragmentation effect also subsides. This explains why the fractal dimension of high-speed debris avalanches remains within a stable range, according to field investigations. Most high-speed debris avalanches exhibit a fractal dimension that falls within the range of 2.3–3.2. To illustrate this point, the fractal dimension of a high-speed rock avalanche is approximately 2.6, and that of a high-speed volcanic avalanche is approximately 2.7 (Crosta et al., 2007).

4.3. Applications and research limitations

This study systematically reveals the dynamic coupling mechanism of frictional weakening and dilatancy effects in granular flow through multi-scale experiments and numerical simulations. It incorporates the temporal and spatial synchronicity of particle collision intensity, dilation, and frictional weakening into a unified analytical framework for the first time, providing critical experimental evidence and theoretical breakthroughs for understanding the extraordinary motion characteristics of high-speed debris avalanches. The present framework primarily focuses on collision-dominated regimes under specific stress levels. The stress level settings in the physical experiments may have a certain application range. In the drum experiment, the centrifugal force can be converted into an effective measure of the applied stress level. When the drum rotates, the centrifugal acceleration experienced by the particles is $a_c = w^2 r$. This acceleration can be equivalently expressed as a magnification of gravitational acceleration: $N = a_c/g$. In the granular system, the normal stress (σ_n) is positively correlated with the equivalent gravity, which can be expressed as

$$\sigma_n = \rho g N H^* \tag{16}$$

The stress levels in the drum experiments were found to fall within the range of 0–20 kPa (Fig. 13a). The pioneering work on the modulation of shear rates in confined flows with fractal particle distributions provides valuable insights for interpreting the observed friction weakening under a wide range of pressure

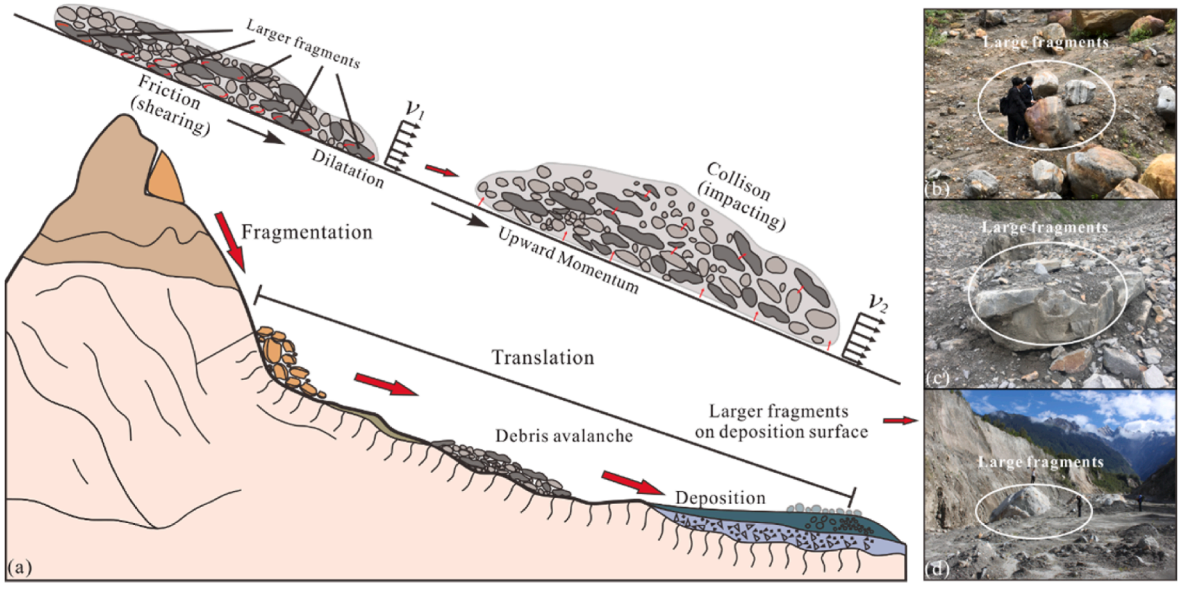

Fig. 12. Mechanism of friction weakening of a high-speed debris avalanche and evidence from field investigation. (a) Large fragments are prone to dilation due to the collision effect, and the contact between the sliding mass and the substrate decreases. Enormous fragments can be widely observed on the surface of the deposition region of (b) the Zelongnong debris avalanche, which occurred in 2018 in Tibet, China; (c) the Xinmo debris avalanche, which occurred in 2017 in Sichuan, China; and (d) the Yigong debris avalanche, which occurred in 2000 in Tibet, China.

conditions (e.g. $P = 1$ kPa, 10 kPa, and 100 kPa; Ding et al., 2024). Our experiments have further refined the gradient of stress levels by conducting 96 loading tests within the stress range of 0–20 kPa, with an average stress increment of 0.2 kPa between each group. This approach allows a more detailed capture of the dynamic changes in the stress-dependent drag reduction effects of debris avalanches under low to medium stress conditions. Additionally, to maximize the relevance of physical experiments to real-world disasters, it is essential to conduct experiments at the largest feasible scale, with the inertial number requirement being in the range of 1×10^{-5} to 1×10^{-1} (Choi et al., 2024). The inertial number I ($I = \dot{\gamma}d/\sqrt{P/\rho}$) was calculated for the drum experiments and found to be below 0.1 in all cases, indicating that the stress levels in the drum experiments can reflect the stress characteristics of actual debris avalanches (Fig. 13b).

Moreover, the research system has established a core correlation model of granular flow dynamics in an idealized setup. It is important to note that the complex topographic boundaries of natural landslides, such as abrupt changes in basal roughness and three-dimensional topographic effects, may modulate the chain response of particle collision and dilatancy. Although the simplification of homogeneous spheres in the numerical model effectively reveals the macroscopic laws of collision energy transfer, further exploration is needed to incorporate the real angular morphology of debris and the dynamic fragmentation processes. The proposed critical threshold value of the Savage number ($N_s > 1.06$) not only provides a quantitative criterion for triggering frictional weakening at the laboratory scale but also establishes a key dimensionless parameter foundation for constructing cross-scale disaster dynamics models in the future. The identified stable interval of debris particle sizes also offers a new physical explanation for the self-organized evolution patterns observed in different types of high-speed debris avalanches.

The primary reason for selecting artificial granular materials was to isolate complex geological factors and focus on the mechanical coupling mechanism of “dilation-driven friction weakening”. Although the surface roughness of natural particles may enhance localized frictional dissipation compared to artificial spherical materials, this effect predominantly governs static or quasi-static frictional strength characteristics. As this study focuses on the inertia-dominated regime, such differences in materials do not compromise the identification of dilation-driven friction reduction as the dominant mechanism. The limitations of this study mainly include two aspects: (1) The complex particle size distribution in natural debris avalanches: polymodal particle distributions in real events may introduce competing effects between segregation-induced lubrication and interlocking resistance. (2) Fragmentation effects: the collision-induced dilation effect is most pronounced in dry granular flows characterized by sufficient kinetic energy to maintain sustained particle saltation. However, its governing influence may become attenuated in fine-grained systems induced by fragmentation. Future research should further investigate the coupled effects of polymodal particle size distributions and fragmentation in natural debris avalanches. Through multiscale simulations and experimental validation, the friction weakening mechanisms governed by the interplay between collisional and viscous effects in complex granular systems could be elucidated, thereby providing more accurate theoretical support for hazard dynamics modeling.

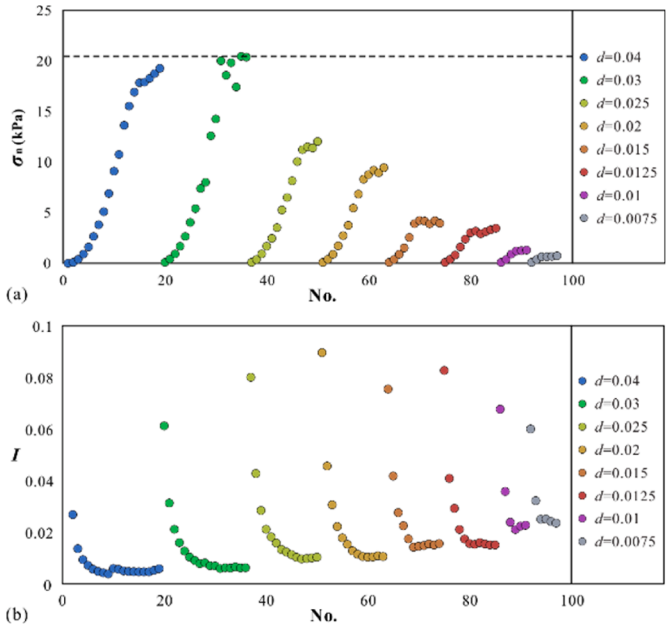

Fig. 13. Dynamic parameters for all test loading groups on the rotation drum experiment: (a) The normal stress; and (b) The inertial number.

5. Conclusions

High-speed debris avalanches typically exhibit pronounced friction weakening effects. The dilation of rock fragments has been observed to synchronize with frictional weakening during such events. This study reveals that the mechanism of friction weakening is driven by particle collisions, which induce dilation in granular flows, thereby resulting in contact between the sliding mass and substrates. The dilation is negatively correlated with the friction coefficient and is influenced by the velocity condition and fragment size. Among these factors, fragment size is identified as the critical influencing factor of friction weakening. Fragment size directly affects the normal force experienced by the sliding mass. Granular flows containing larger fragments show a more rapid reduction in normal force. The critical condition for triggering friction weakening in debris avalanches has been found to be a fractal dimension $D < 2.65$, as supported by physical experimental data. In such conditions, the peak Savage number exceeds 1.06, thereby enabling the collision effect to gradually dominate as velocity increases. This ultimately leads to friction weakening. Finally, a mathematical model was developed, based on the granular inertial collision–friction coupling equation, to quantitatively describe the relationships among collisions, dilation, and friction weakening.

CRediT authorship contribution statement

Yuxiang Hu: Writing – original draft, Validation, Methodology, Investigation, Formal analysis. **Congjiang Li:** Validation, Investigation, Formal analysis. **Qingyang Zhu:** Visualization, Investigation, Data curation. **Haibo Li:** Validation, Software, Funding acquisition, Formal analysis. **Jiawen Zhou:** Writing – review & editing, Supervision, Resources, Project administration, Funding acquisition, Conceptualization.

Declaration of competing interest

The authors declare that they have no known competing financial interests or personal relationships that could have appeared to influence the work reported in this paper.

Acknowledgement

This work was supported by the National Natural Science Foundation of China (Grant Nos. U2240221 and 52379105) and the National Key R&D Program of China (Grant No. 2022YFC3080100). Critical comments by the anonymous reviewers greatly improved the initial manuscript.

Appendices A–C. Supplementary data

Supplementary data to this article can be found online at https://doi.org/10.1016/j.jrmge.2025.08.010.

References

Allstadt, K.E., Farin, M., Iverson, R.M., et al., 2019. Measuring basal force fluctuations of debris flows using seismic recordings and empirical Green's functions. J. Geophys. Res.: Earth Surf. 125, e2020JF005590.

Bartali, R., Molinari, Y.N., Linán, G.M.R., Cisneros, L.A.T., Ángle, G.P., 2020. Gravity-driven monodisperse avalanches: inertial to frictional-dominated flow. Rock Mech. Rock Eng. 53, 3507–3520.

Cagnoli, B., Romano, G.P., 2012. Effects of flow volume and grain size on mobility of dry granular flows of angular rock fragments: a functional relationship of scaling parameters. J. Geophys. Res. Solid Earth 117. https://doi.org/10.1029/2011JB008926.

Campbell, C.S., 1989. Self-Lubrication for long runout landslides. J. Geol. 97, 653–665.

Choi, C.E., Ng, C.W.W., Liu, H., 2024. Flume modeling of debris flows. In: Jakob, M., McDougall, S., Santi, P. (Eds.), Advances in debris-flow Science and Practice. Geoenvironmental Disaster Reduction. Springer, Cham, Switzerland, pp. 93–125.

Collins, G., Melosh, H.J., 2003. Acoustic fluidization and the extraordinary mobility of sturzstroms. J. Geophys. Res. Solid Earth 108. https://doi.org/10.1029/2003JB002465.

Crosta, G.B., Frattini, P., Fusi, N.C., 2007. Fragmentation in the Val Pola rock avalanche, Italian Alps. J. Geophys. Res.: Earth Surf. 112. https://doi.org/10.1029/2005JF000455.

Cruden, D.M., Hungr, O., 1986. The debris of the Frank Slide and theories of rockslide-avalanche mobility. Can. J. Earth Sci. 23, 425–432.

Cruden, D.M., Krahn, J.P., 1978. Chapter 2-Frank rockslide, Alberta, Canada. Dev. Geotech. Eng. 14, 97–112.

Davies, T.R., 1982. Spreading of rock avalanche debris by mechanical fluidization. Rock Mech. 15, 9–24.

Davies, T.R., McSaveney, M., 1999. Runout of dry granular avalanches. Can. Geotech. J. 36, 313–320.

Davies, T.R., McSaveney, M., 2009. The role of rock fragmentation in the motion of large landslides. Eng. Geol. 109, 67–79.

Deline, P., Alberto, W., Broccolato, M., Hungr, O., Noetzli, J., Ravanel, L., Tamburini, A., 2011. The December 2008 Crammont rock avalanche, Mont Blanc massif area, Italy. Nat. Hazards and Earth. Syst. Sci. 11, 3307–3318.

Deng, Y., Fan, X., Scaringi, G., Wang, D., He, S., 2023. Effect of particle crushing- and thermally induced pressurization on rockslide mobility. Landslides 20, 1535–1546.

Ding, Z.W., Hu, W., Chang, C.S., Li, Yan, Wang, G.H., 2024. Shear behaviors of confined flow: insights for understanding the influences of fractal particle size distribution on high mobility of granular flows. Geophys. Res. Lett. 51, e2024GL108956.

Fisher, R.V., 1971. Features of coarse-grained, high-concentration fluids and their deposits. J. Sediment. Res. 41, 916–927.

Frattini, P., Crosta, G.B., 2013. The role of material properties and landscape morphology on landslide size distributions. Earth Planet Sci. Lett. 361, 310–319.

Goren, L., Aharonov, E., 2007. Long runout landslides: the role of frictional heating and hydraulic diffusivity. Geophys. Res. Lett. 34. https://doi.org/10.1029/2006GL028895.

Hsu, L., Dietrich, W.E., Sklar, L.S., 2008. Experimental study of bedrock erosion by granular flows. J. Geophys. Res.: Earth Surf. 113. https://doi.org/10.1029/2007JF000778.

Hu, W., Huang, R., McSaveney, M., Zhang, X., Yao, L., Shimamoto, T., 2018. Mineral changes quantify frictional heating during a large low-friction landslide. Geology 46, 223–226.

Iverson, R.M., Vallance, J.W., 2001. New views of granular mass flows. Geology 29, 115–118.

Johnson, B.C., Campbell, C.S., Melosh, H.J., 2015. The reduction of friction in long runout landslides as an emergent phenomenon. J. Geophys. Res.: Earth Surf. 121, 881–889.

Lai, Z., Vallejo, L.E., Zhou, W., Ma, G., Espitia, J.M., Caicedo, B., Chang, X., 2017. Collapse of granular columns with fractal particle size distribution: implications for understanding the role of small particles in granular flows. Geophys. Res. Lett. 44, 12181–12189.

Legros, F., 2002. The mobility of long-runout landslides. Eng. Geol. 63, 301–331.

Li, G.K., Moon, S., 2021. Topographic stress control on bedrock landslide size. Nat. Geosci. 14, 307–14313.

Lucas, A.S., Mangeney, A., Ampuero, J.P., 2014. Frictional velocity-weakening in landslides on Earth and on other planetary bodies. Nat. Commun. 5, 3417.

McEwen, A.S., 1989. Mobility of large rock avalanches: evidence from Valles Marineris. Mars. Geol. 17, 1111–1114.

Medwedeff, W.G., Clark, M.K., Zekkos, D., West, A.J., 2020. Characteristic landslide distributions: an investigation of landscape controls on landslide size. Earth Planet. Sci. Lett. 539, 116203.

Mindlin, R.D., Deresiewicz, H., 1953. Elastic spheres in contact under varying oblique force. J. Appl. Mech. 20, 327–344.

Robinson, T.R., Davies, T., Reznichenko, N.V., De Pascale, G.P., 2015. The extremely long-runout Komansu rock avalanche in the Trans Alai range, Pamir Mountains, Southern Kyrgyzstan. Landslides 12, 523–535.

Singer, K.N., McKinnon, W.B., Schenk, P.M., Moore, J.M., 2012. Massive ice avalanches on Iapetus mobilized by friction reduction during flash heating. Nat. Geosci. 5, 574–578.

Stark, C.P., Hovius, N., 2001. The characterization of landslide size distributions. Geophys. Res. Lett. 28, 1091–1094.

Staron, L., Hinch, E.J., 2007. The spreading of a granular mass: role of grain properties and initial conditions. Granul. Matter 9, 205–217.

Walker, D.M., Tordesillas, A., 2010. Topological evolution in dense granular materials: a complex networks perspective. Int. J. Solid Struct. 47, 624–639.

Yamada, M., Mangeney, A., Matsushi, Y., Matsuzawa, T., 2018. Estimation of dynamic friction and movement history of large landslides. Landslides 15, 1963–1974.

Zhao, S., He, S., Li, X., Deng, Y., Liu, Y., Yan, S., Bai, X., Xie, Y., 2021. The Xinmo rockslide-debris avalanche: an analysis based on the three-dimensional material point method. Eng. Geol. 287, 106109.

Yuxiang Hu obtained his MSc and PhD degrees from Sichuan University in China in 2020 and 2023, respectively. Since 2023, he has been affiliated with Sichuan University, as an assistant researcher. His research focuses on landslide disaster mechanisms and mitigation strategies, with particular expertise in the following areas: (1) the dynamic processes governing high-speed long-runout landslides, (2) advanced numerical modeling for hazard prediction and risk assessment, and (3) the development of engineering solutions for cascading geological disasters in mountainous terrain. This research integrates field investigations, computational mechanics, and geotechnical engineering approaches to enhance disaster resilience.